Preprints, Second IFAC Modeling, Estimation and Control Conference
October 2-5, 2022. Jersey City, New Jersey, USA
Preprints, IFAC MECC 2022
October 2-5, 2022. Jersey City, New Jersey, USA

Non-Causal State Estimation for Improved State Tracking in Iterative Learning Control

Kentaro Tsurumoto * **Wataru Ohnishi** * **Takafumi Koseki** *
Nard Strijbosch ** **Tom Oomen** **,***

* *Department of Electrical Engineering and Information Systems, The University of Tokyo, Tokyo, Japan*
(e-mail: tsuruken@koseki.t.u-tokyo.ac.jp).
** *Department of Mechanical Engineering, Eindhoven University of Technology, 5600 MB Eindhoven, The Netherlands*
*** *Faculty of Mechanical, Maritime, and Materials Engineering, Delft University of Technology, 2628 CD Delft, The Netherlands*

Abstract:
State-tracking Iterative Learning Control (ILC) yields perfect state-tracking performance at each n sample instances for systems that perform repetitive tasks, where n stands for the order of the system. By achieving perfect state-tracking, oscillatory intersample behavior often encountered in output-tracking ILC has been mitigated. However, state-tracking ILC only assures the estimated state error to converge to a significantly small value, meaning the accuracy of the state estimation takes a critical role. State estimation using a causal state observer has had an inevitable trade-off between the estimation delay and the noise sensitivity. By utilizing the non-causal operation of ILC, a non-causal state estimation can be designed. This non-causal state estimation performs beyond the trade-off of causal estimation, improving the estimation delay without compromising the noise sensitivity. The aim of this paper is to implement the non-causal state observer to state-tracking ILC, and present the improved state tracking by applying it to a second order system.

Keywords: Iterative Learning Control, State Observer, Kalman Smoothing, Stable Inversion

1. INTRODUCTION

Iterative Learning Control (ILC) is a method which can significantly improve the control performance in repetitive tasks. By learning from the positioning error of the previous iteration, the control input of the next iteration is updated. This results to exponentially less positioning error per iteration, leading to theoretical perfect tracking when repeated enough times under negligible iteration varying disturbance. Therefore, ILC has been widely applied to precision machinery such as semiconductor lithography systems (Van Der Meulen et al., 2008; Mishra et al., 2007), machine tools (Hayashi et al., 2020), industrial printers (Oomen, 2018), mechatronic imaging systems (Csencsics et al., 2019), and industrial robots (Wallén et al., 2011).

Due to the learning process, ILC has enabled a more accurate and faster on-sample output-tracking than feedback (FB) and feedforward (FF) in the discrete-time domain. One design procedure for ILC is a frequency domain design (frequency domain ILC (Bristow et al., 2006)). To achieve fast convergence and high asymptotic performance, the learning filter is designed as an accurate inverse model of the system. For system inversion, a stable inversion technique with preactuation is widely employed (Van Zundert and Oomen, 2018).

Such output-tracking ILC can achieve high-tracking performance on-sample, poor inter-sample behaviors are often observed. Inter-sample positioning performance can not be dismissed because manufacturing processes, for example, exposure or milling, are performed in continuous-time domain.

To address this problem, an ILC framework focusing on tracking the state variable of the controlled system (state-tracking ILC) has been proposed (Ohnishi et al., 2021). This method is motivated by the concept of multirate feedforward control (Fujimoto et al., 2001; Ohnishi et al., 2019), which achieves not only output tracking but also state tracking.

Although state-tracking ILC has improved the inter-sample behavior, the benefit of utilizing non-causal estimators has not yet been explored. Causal state observers have fundamental trade-offs between estimation delay and the noise sensitivity, leading to inevitable state estimation error. The aim of this paper is to present an approach which takes full advantage of the non-causal state observer, achieving better state tracking results than the state-tracking ILC with causal observer.

Contributions of this paper are as follows:

- C1 In Section 3, the basic idea of applying a non-causal state observer leading to a better state tracking performance is presented.
- C2 In Section 4, the design procedure of a non-causal state observer is presented. The design is extended from a causal state observer without requiring any additional information of the system.
- C3 In Section 5, simulation verification is demonstrated through a second order system, showing improved on-sample state tracking performance.

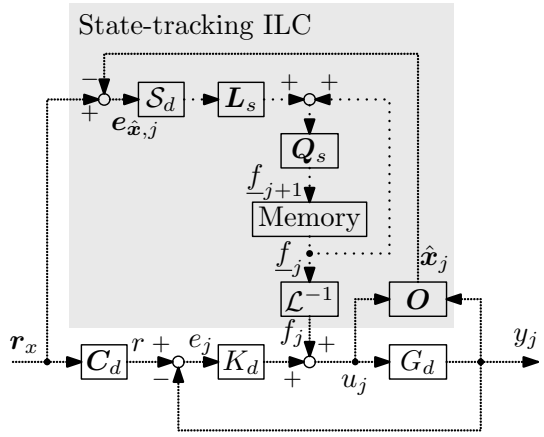

Fig. 1. Block diagram of state tracking ILC. The high-frequency dots and low-frequency dots denote high-rate signal sampled by T_s and slow-rate signal sampled by nT_s, respectively.

1.1 Notations

Let $G_d(z)$ denote a discrete-time, linear time-invariant single-input single-output (SISO) system with n state variables, expressed as

$$G_d = \boldsymbol{C}_d(z\boldsymbol{I} - \boldsymbol{A}_d)^{-1}\boldsymbol{B}_d + D_d \overset{z}{\coloneqq} \left[\begin{array}{c|c} \boldsymbol{A}_d & \boldsymbol{B}_d \\ \hline \boldsymbol{C}_d & D_d \end{array}\right], \tag{1}$$

where $\boldsymbol{A}_d \in \mathbb{R}^{n\times n}$, $\boldsymbol{B}_d \in \mathbb{R}^{n\times 1}$, $\boldsymbol{C}_d \in \mathbb{R}^{1\times n}$, $D_d \in \mathbb{R}$.

Definition 1 (Discrete-time lifting)**.** *Let $u[k] \in \mathbb{R}$ and lifted signal over n samples is denoted as $\underline{u}[l] = \mathcal{L}u[k]$ with*

$$\underline{u}[l] = \begin{bmatrix} u[ln] & u[ln+1] & \cdots & u[ln+n-1] \end{bmatrix}^\top \in \mathbb{R}^n, \tag{2}$$

where $l \in \mathbb{Z}$ and $\mathcal{L}$ denotes lifting operator, which maps $u \mapsto \underline{u}$. An inverse lifting operator is given by $u = \mathcal{L}^{-1}\underline{u}$.

Definition 2 (Lifted system in state space)**.** *The input/output of lifted system of G_d over n samples would be $\underline{y} = \mathcal{L}y = (\mathcal{L}G_d\mathcal{L}^{-1})(\mathcal{L}u) = \underline{G_d}\underline{u}$.*

Definition 3 (Downsampling operator)**.** *The downsampling operation over n samples is defined by $y[kn] = \mathcal{S}_d(y[k])$.*

Assumption 1 (Controlled continuous-time system G)**.** *A controlled system $G = \boldsymbol{C}(s\boldsymbol{I} - \boldsymbol{A})^{-1}\boldsymbol{B}$ is a continuous-time SISO, strictly proper, linear-time invariant system given by minimal realization.*

The discrete-time system G_d of G by using zero-order hold with sampling period T_s is denoted as

$$\begin{aligned} \boldsymbol{x}[k+1] &= \boldsymbol{A}_d\boldsymbol{x}[k] + \boldsymbol{B}_d u[k], \\ y[k] &= \boldsymbol{C}_d\boldsymbol{x}[k], \end{aligned} \tag{3}$$

where $k \in \mathbb{Z}$, $\boldsymbol{x}[k] \in \mathbb{R}^n$, $u[k], y[k] \in \mathbb{R}$, $\boldsymbol{x}[k]$, $y[k]$, and $u[k]$ correspond to $\boldsymbol{x}(kT_s)$, $y(kT_s)$, and $u(kT_s)$ respectively.

2. STATE-TRACKING ILC

In this section, the state-tracking error of state-tracking ILC is formulated. First, in Section 2.1, the frequency domain design of state-tracking ILC is introduced (Ohnishi et al., 2021). Then, Section 2.2 presents the problem formulation of the state-tracking error caused by the state-tracking ILC framework.

2.1 Frequency domain ILC for state tracking

The aim of state-tracking ILC is to achieve perfect state tracking at every n sampling instances for systems that perform repetitive tasks, where n stands for the number of the system's state variables. It updates feedforward input over iterations through learning from the estimated state tracking error in the past iteration. An advantage in the design aspect is by making use of non-parametric frequency-domain measurements, the robustness of learning can be guaranteed with limited user effort. See Ohnishi et al. (2021) for further details.

The block diagram of state-tracking ILC is shown in Fig. 1. It has two sampling rates in the signal: 1) T_s drawn as high-frequency dots is the high-rate, which is the same as the rate of control input and measurement, and 2) nT_s drawn as low-frequency dots is the low-rate in the lifted domain.

$\boldsymbol{r}_x$ in Fig. 1 denotes the state trajectory to be tracked by the state-tracking ILC with the following assumption.

Assumption 2 (State trajectory $\boldsymbol{r}_x$)**.** *State trajectory $\boldsymbol{r}_x \in \mathbb{R}^n$ that satisfies*

$$r[k] = \boldsymbol{C}_d\boldsymbol{r}_x[k], \quad \forall k, \tag{4}$$

is pre-determined.

To achieve state-tracking, a state observer $\boldsymbol{O}$ is employed to obtain the state estimation $\hat{\boldsymbol{x}}_j$ of the system. State tracking error estimate $\boldsymbol{e}_{\hat{\boldsymbol{x}},j}$ is defined as next.

Definition 4 (State tracking error estimate)**.** *State tracking error estimate $\boldsymbol{e}_{\hat{\boldsymbol{x}},j} \in \mathbb{R}^n$ at j-th iteration is obtained by*

$$\boldsymbol{e}_{\hat{\boldsymbol{x}},j} = \boldsymbol{r}_x - \hat{\boldsymbol{x}}_j, \tag{5}$$

where $\hat{\boldsymbol{x}}_j \in \mathbb{R}^n$ denotes the state estimate made by the state observer $O \in \mathcal{RL}_\infty^{n\times 2}$ at the j-th iteration

$$\hat{\boldsymbol{x}}_j = \boldsymbol{O}\begin{bmatrix} u_j \\ y_j \end{bmatrix}, \tag{6}$$

where u_j denotes control input of G_d which consists of feedforward input from the learning filter and feedback input from feedback controller K_d.

A learning filter and a robustness filter in the lifted domain is applied to $\boldsymbol{e}_{\hat{\boldsymbol{x}},j}$ to achieve better state-tracking in the next iteration. Lifted ILC force for the $j+1$-th iteration $\underline{f}_{j+1} \in \mathbb{R}^n$ is updated from the j-th iteration as defined in next.

Definition 5 (State-tracking ILC force update)**.**

$$\underline{f}_{j+1} = \boldsymbol{Q}_s(\underline{f}_j + \boldsymbol{L}_s\boldsymbol{e}_{\hat{\boldsymbol{x}},j}), \tag{7}$$

where $\boldsymbol{Q}_s \in \mathcal{RL}_\infty^{n\times n}$ and $\boldsymbol{L}_s \in \mathcal{RL}_\infty^{n\times n}$ denotes the robustness filter and the learning filter, respectively. Note that non-causal operation is allowed for $\boldsymbol{Q}_s$ and $\boldsymbol{L}_s$ since $\underline{f}_{j+1}$ is only needed before the $j+1$-th iteration starts.

To derive the relationship between the state tracking error estimate $\boldsymbol{e}_{\hat{\boldsymbol{x}},j}$, lifted state reference $\underline{\boldsymbol{r}_x}$, and lifted ILC force $\underline{f}_j$, Definition 6 and Definition 7 are formulated.

Definition 6 (Lifted state reference $\underline{\boldsymbol{r}_x}$ and lifted reference $\underline{r}$)**.** *The lifted state reference $\underline{\boldsymbol{r}_x}$ and lifted reference $\underline{r}$ satisfy*

$$\underline{r} = (\boldsymbol{I}_n \otimes \boldsymbol{C}_d)\underline{\boldsymbol{r}_x} \coloneqq \underline{\boldsymbol{C}_d}\,\underline{\boldsymbol{r}_x}, \tag{8}$$

where $\boldsymbol{I}_n$ and $\otimes$ denote n-by-n identity matrix and the Kronecker tensor product, respectively.

Definition 7 (State selection matrix $\mathcal{S}$)**.** *The state selection matrix $\mathcal{S}$ selects the first sample elements from the lifted signal.*

$$\mathcal{S} = \begin{bmatrix} \boldsymbol{I}_n & \boldsymbol{0}_{n\times n(n-1)} \end{bmatrix} \in \mathbb{R}^{n\times n^2}, \tag{9}$$

where $\boldsymbol{0}_{n\times n(n-1)}$ denotes n-by-$n(n-1)$ matrix of zeros.

From the aforementioned definitions, a fundamental equation stating the relationship between the state tracking error estimate $\boldsymbol{e}_{\hat{\boldsymbol{x}},j}$, lifted state reference $\underline{\boldsymbol{r}_x}$, and lifted ILC force $\underline{f}_j$ is derived.

Lemma 1 (State tracking error estimate $\boldsymbol{e}_{\hat{\boldsymbol{x}},j}$ in lifted domain (Ohnishi et al., 2021))**.**

$$\mathcal{S}_d \boldsymbol{e}_{\hat{\boldsymbol{x}},j} = \boldsymbol{S}_x \underline{\boldsymbol{r}_x} - \boldsymbol{J}_x \underline{f}_j, \tag{10}$$

where

$$\boldsymbol{S}_x \coloneqq \mathcal{S}(\boldsymbol{I} - \underline{\boldsymbol{G}_o K_d S\, C_d}) \in \mathcal{RL}_\infty^{n\times n^2}, \tag{11}$$

$$\boldsymbol{J}_x \coloneqq \mathcal{S}\underline{\boldsymbol{G}_o S} \in \mathcal{RL}_\infty^{n\times n}, \tag{12}$$

and $S = (I + G_d K_d)^{-1}$ denotes the sensitivity function of the closed-loop system, $\boldsymbol{G}_o \in \mathcal{RL}_\infty^{n\times 1}$ denotes a transfer function from the control input u_j to state estimate $\hat{\boldsymbol{x}}_j$ as following.

$$\hat{\boldsymbol{x}}_j = \boldsymbol{O}\begin{bmatrix} u_j \\ y_j \end{bmatrix} = \boldsymbol{O}\begin{bmatrix} u_j \\ G_d u_j \end{bmatrix} = \boldsymbol{O}\begin{bmatrix} I \\ G_d \end{bmatrix} u_j \coloneqq \boldsymbol{G}_o u_j. \tag{13}$$

Proof. See Ohnishi et al. (2021). □

Using Definition 5 and Lemma 1, the propagation of state tracking error and lifted ILC force per iteration can be formulated as following.

Lemma 2 (State tracking error and force propagation (Ohnishi et al., 2021))**.** *State tracking error and lifted ILC force propagation are formulated as*

$$\mathcal{S}_d \boldsymbol{e}_{\hat{\boldsymbol{x}},j+1} = \boldsymbol{J}_x \boldsymbol{Q}_s (\boldsymbol{I} - \boldsymbol{L}_s \boldsymbol{J}_x) \boldsymbol{J}_x^{-1} \mathcal{S}_d \boldsymbol{e}_{\hat{\boldsymbol{x}},j} + (\boldsymbol{I} - \boldsymbol{J}_x \boldsymbol{Q}_s \boldsymbol{J}_x^{-1}) \boldsymbol{S}_x \underline{\boldsymbol{r}_x}, \tag{14}$$

$$\underline{f}_{j+1} = \boldsymbol{Q}_s (\boldsymbol{I} - \boldsymbol{L}_s \boldsymbol{J}_x) \underline{f}_j + \boldsymbol{Q}_s \boldsymbol{L}_s \boldsymbol{S}_x \underline{\boldsymbol{r}_x}. \tag{15}$$

Proof. Follow from substitution of Lemma 1 to Definition 5. □

By defining the convergence of lifted ILC force $\underline{f}$ as Definition 8, the convergence condition of (14) and (15) can be given as Lemma 3.

Definition 8 (lifted ILC force convergence)**.** *The system of (15) is convergent if and only if for all $\underline{\boldsymbol{r}_x}, \underline{f}_j \in \ell_2$, there exists an asymptotic signal $\underline{f}_\infty \in \ell_2$ such that*

$$\lim_{j\to\infty} \sup \left\| \underline{f}_\infty - \underline{f}_j \right\|_{\ell_2} = 0. \tag{16}$$

Lemma 3 (Convergence condition (Ohnishi et al., 2021))**.** *The iteration (14) and (15) converge if and only if*

$$\rho\left(\boldsymbol{Q}_s(e^{i\omega})(\boldsymbol{I} - \boldsymbol{L}_s(e^{i\omega})\boldsymbol{J}_x(e^{i\omega}))\right) < 1, \quad \forall \omega \in [0, \pi], \tag{17}$$

where $\rho(\cdot)$ denotes the spectral radius, i.e $\rho(\cdot) = \max_i |\lambda_i(\cdot)|$.

Proof. Can be proved by the use of Parseval's identity. See Norrlöf and Gunnarsson (2002) for further details. □

The important aspect of the state-tracking ILC in frequency domain design is that the condition in (17) can be verified by a measured frequency response data of G_d and S, which is fast, accurate, and inexpensive. This leads to a limited design effort for the user.

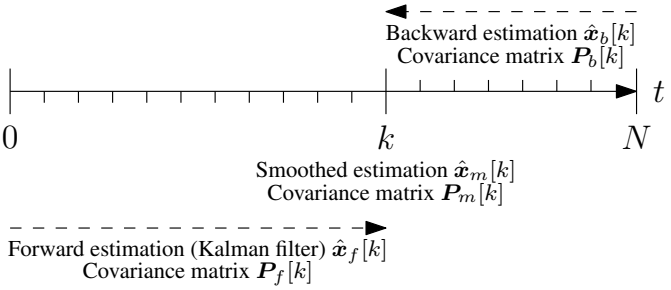

Fig. 2. Basic concept of fixed-interval smoothing. By combining $\hat{\boldsymbol{x}}_f$ and $\hat{\boldsymbol{x}}_b$, a smoothed estimate $\hat{\boldsymbol{x}}_m$ is achieved.

From (14) and (15), the asymptotic signals $\boldsymbol{e}_{\hat{\boldsymbol{x}},\infty}$ and $\underline{f}_\infty$ are obtained as

$$\mathcal{S}_d \boldsymbol{e}_{\hat{\boldsymbol{x}},\infty} = \left(\boldsymbol{I} - \boldsymbol{J}_x(\boldsymbol{I} - \boldsymbol{Q}_s(\boldsymbol{I} - \boldsymbol{L}_s\boldsymbol{J}_x))^{-1}\boldsymbol{Q}_s\boldsymbol{L}_s\right)\boldsymbol{S}_x\underline{\boldsymbol{r}_x}, \tag{18}$$

$$\underline{f}_\infty = (\boldsymbol{I} - \boldsymbol{Q}_s(\boldsymbol{I} - \boldsymbol{L}_s\boldsymbol{J}_x))^{-1}\boldsymbol{Q}_s\boldsymbol{L}_s\boldsymbol{S}_x\underline{\boldsymbol{r}_x}. \tag{19}$$

The requirement for $\boldsymbol{Q}_s$ to achieve zero asymptotic estimated state tracking error is given in Lemma 4. In addition, (14) and (18) motivate to design the learning filter as $\boldsymbol{L}_s = \boldsymbol{J}_x^{-1}$ to achieve fast convergence.

Lemma 4 (Requirement for $\boldsymbol{Q}_s$ for $\mathcal{S}_d \boldsymbol{e}_{\hat{\boldsymbol{x}},\infty} = 0$ (Ohnishi et al., 2021))**.** *Assume $\boldsymbol{L}_s(e^{i\omega}), \boldsymbol{J}_x(e^{i\omega}) \neq 0, \forall\omega$. Given that (17) holds, for all $\boldsymbol{r}_x \in \ell_2, \mathcal{S}_d \boldsymbol{e}_{\hat{\boldsymbol{x}},\infty} = 0$, if and only if $\boldsymbol{Q}_s = \boldsymbol{I}_n$.*

Proof. See Ohnishi et al. (2021). □

To summarize, the state-tracking ILC has three main favorable properties: 1) a trial domain stability condition (17) available, 2) limited design effort using non-parametric model, and 3) perfect state tracking per n samples (Lemma 4). However, there is one major downside in this method and this would be formulated in the following subsection.

2.2 Problem Formulation

The problem addressed in this paper is to improve the state tracking error performance of the state-tracking ILC.

Note that as defined in Definition 4, even when requirements in Lemma 4 are satisfied, state-tracking ILC only assures the estimated state $\hat{\boldsymbol{x}}$ to perfectly track the state trajectory $\boldsymbol{r}_x$. Therefore, the accuracy of $\hat{\boldsymbol{x}}$ heavily effects the performance. This means that improving the state estimation can directly improve the performance of state-tracking ILC. In causal operation, without a perfect modelling of the plant G_d, there is always an estimation delay. Faster estimation can be performed by using a higher bandwidth state observer, but this comes with the cost of an estimation more susceptible to noise.

The aim of this paper is to investigate an effective non-causal approach for state estimation and implement it to state-tracking ILC. By utilizing the non-causality, more measurement data are used for the estimation, resulting to a better state estimation and state tracking performance.

3. CONCEPTUAL IDEA

In this section, the idea of an effective non-causal state observer is presented.

3.1 Effective offline state estimation

One major option for offline state estimation is fixed-interval smoothing (Simon, 2006; Anderson and Moore, 2005). Fixed-interval smoothing is a Kalman smoothing method which can be applied when all $N \in \mathbb{N}$ samples of the measurement data are provided beforehand. It obtains a state estimation by combining a forward estimation and backward estimation as in Fig. 2. However, as time k of the estimation comes closer to N, the backward estimation becomes more unreliable.

To address this problem, assuming converged states for the beginning and end of the plant, a novel backward estimation method of applying stable inversion (Van Zundert and Oomen, 2018) to state estimation is presented. In this paper, fixed-interval smoothing utilizing the backward estimation method is referred as the non-causal state observer.

4. DESIGN OF NON-CAUSAL STATE OBSERVER

In this section, the design procedure of the non-causal state observer is presented. By combining a forward estimation (Section 4.2) and backward estimation (Section 4.3), a non-causal state estimation (Section 4.4) is achieved.

The followings are assumed in this section.

Definition 9 (Apriori and aposteriori estimations)**.** *A state estimation obtained at time k based on measurements up to time j is described as, $\hat{x}[k \mid j] = E(x[k] \mid y[1], \cdots, y[j])$. An* apriori *estimate is based on measurements up to time $k-1$, and an* aposteriori *estimate is based on measurements up to time k, which are same to $\hat{x}[k \mid k-1]$ and $\hat{x}[k \mid k]$, respectively.*

Lemma 5 (Full-order state observer)**.** *The state estimation results obtained by a causal full-order state observer is an* apriori *estimate.*

Proof. From the state equation of a discrete time full-order state observer (20), the state estimation of time k is calculated only by measurements up to time $k-1$.

$$\begin{aligned} \hat{\boldsymbol{x}}[k] &= \boldsymbol{A}_d \hat{\boldsymbol{x}}[k-1] + \boldsymbol{B}_d u[k-1] + \boldsymbol{H}(y[k-1] - \hat{y}[k-1]), \\ \hat{y}[k-1] &= \boldsymbol{C}_d \hat{\boldsymbol{x}}[k-1]. \end{aligned} \tag{20}$$

where $\boldsymbol{H}$ denotes the observer gain of the state observer. □

This paper mainly introduces four state estimation methods. The forward apriori estimate, forward aposteriori estimate, backward apriori estimate, and mixed non-causal estimate. Symbols are notified by using the subscript o, f, b, m, respectively.

Remark 1. *For full use of the whole N sample of measurement data, the mixed non-causal estimate $\hat{x}_m$ is composed by the forward* aposteriori *estimate $\hat{x}_f = E(x[k] \mid y[1], \cdots, y[k])$ and the backward* apriori *estimate $\hat{x}_b = E(x[k] \mid y[k+1], \cdots, y[N])$.*

4.1 Identification of the Discrete time plant, System noise, and Measurement noise

The first step of designing a non-causal state observer is to identify the discrete time plant $G_d = \boldsymbol{C}_d(z\boldsymbol{I} - \boldsymbol{A}_d)^{-1}\boldsymbol{B}_d + D_d$, and set the covariance matrix of the system noise $\boldsymbol{M}$ and measurement noise N. $\boldsymbol{M}$ and N are tuning factors decided by the designer, determining the bandwidth of the state observer. By solving the Discrete-time Algebraic Riccati Equation (21), the observer gain $\boldsymbol{H}$ can be designed.

$$\boldsymbol{A}_d \boldsymbol{X} \boldsymbol{A}_d^\top - \boldsymbol{X} - \boldsymbol{A}_d \boldsymbol{X} \boldsymbol{C}_d^\top (\boldsymbol{C}_d \boldsymbol{X} \boldsymbol{C}_d^\top + N)^{-1} \boldsymbol{C}_d \boldsymbol{X} \boldsymbol{A}_d^\top + \boldsymbol{M} = 0. \tag{21}$$

Example 1 (Bandwidth of a state observer)**.** *Consider a nominal system $G_n = \frac{0.82224(z+0.9022)}{(z-1)(z-0.7341)}$ with sampling time $T_s = 0.01$ s. The discretized system by zero-order-hold assuming controllable canonical form would be,*

$$G_n = \left[\begin{array}{c|c} \boldsymbol{A}_n & \boldsymbol{B}_n \\ \hline \boldsymbol{C}_n & D_n \end{array}\right] = \left[\begin{array}{cc|c} 1 & 0.0086 & 0.8222 \\ 0 & 0.7341 & 156.4035 \\ \hline 1 & 0 & 0 \end{array}\right].$$

By setting $\boldsymbol{M} = \mathrm{diag}(10^{-6}, 1)$, $N = 10^{-6}$, the bandwidth of the state observer is 37 Hz

4.2 Forward estimation

The forward estimation $\hat{\boldsymbol{x}}_f$ is obtained from a causal state observer. By using the positive definite solution $\boldsymbol{X}^+$ of (21), the observer gain of the causal state observer $\boldsymbol{H}_o$ is calculated as

$$\boldsymbol{H}_o = \boldsymbol{A}_d \boldsymbol{X}^+ \boldsymbol{C}_d^\top (\boldsymbol{C}_d \boldsymbol{X}^+ \boldsymbol{C}_d^\top + N)^{-1}. \tag{22}$$

From (20), the causal state estimation $\hat{\boldsymbol{x}}_o$ is obtained. The covariance matrix of the estimation error for the causal state observer is $\boldsymbol{P}_o = \boldsymbol{X}^+$.

By using the following Lemma 6, the forward estimation $\hat{\boldsymbol{x}}_f$ and covariance matrix of the estimation error $\boldsymbol{P}_f$ is determined.

Lemma 6 (Forward aposteriori estimation and covariance matrix)**.** *The forward aposteriori estimation and covariance matrix of the estimation error are formulated as*

$$\hat{\boldsymbol{x}}_f = \hat{\boldsymbol{x}}_o + \boldsymbol{K}_g(y - \boldsymbol{C}_d \hat{\boldsymbol{x}}_o), \tag{23}$$

$$\boldsymbol{P}_f = (\boldsymbol{I} - \boldsymbol{K}_g \boldsymbol{C}_d)\boldsymbol{P}_o, \tag{24}$$

where $\boldsymbol{K}_g$ denotes the Kalman gain defined by, $\boldsymbol{K}_g = \boldsymbol{A}_d^{-1}\boldsymbol{H}_o$.

Proof. See literature Simon (2006); Anderson and Moore (2005). □

4.3 Backward estimation

The backward estimation $\hat{\boldsymbol{x}}_b$ is obtained by applying stable inversion (Van Zundert and Oomen, 2018) to an unstable state observer, which has the *same bandwidth* as the causal state observer. By using the negative definite solution $\boldsymbol{X}^-$ of (21), the observer gain of the backward state observer $\boldsymbol{H}_b$ is calculated as

$$\boldsymbol{H}_b = \boldsymbol{A}_d \boldsymbol{X}^- \boldsymbol{C}_d^\top (\boldsymbol{C}_d \boldsymbol{X}^- \boldsymbol{C}_d^\top + N)^{-1}. \tag{25}$$

By calculating the state equation backwards as in (26), the backward state estimation $\hat{\boldsymbol{x}}_b$ is obtained.

$$\begin{aligned} \hat{\boldsymbol{x}}_b[k] &= \boldsymbol{A}_d^{-1}\left(\hat{\boldsymbol{x}}_b[k+1] - \boldsymbol{B}_d u[k] - \boldsymbol{H}_b(y[k] - \hat{y}[k])\right), \\ \hat{y}[k] &= \boldsymbol{C}_d \hat{\boldsymbol{x}}_b[k]. \end{aligned} \tag{26}$$

The covariance matrix of the estimation error of backward state observer $\boldsymbol{P}_b$ is determined by the following Lemma 7.

Lemma 7 (Covariance matrix of the backward state observer)**.** *The covariance matrix of the estimation error of backward state observer $\boldsymbol{P}_b$ is the positive definite solution of the following Discrete-time Algebraic Riccati Equation,*

$$\boldsymbol{A}_d' \boldsymbol{X} \boldsymbol{A}_d'^\top - \boldsymbol{X} - \boldsymbol{A}_d' \boldsymbol{X} \boldsymbol{C}_d^\top (\boldsymbol{C}_d \boldsymbol{X} \boldsymbol{C}_d^\top + N)^{-1} \boldsymbol{C}_d \boldsymbol{X} \boldsymbol{A}_d'^\top + \boldsymbol{M}' = 0, \tag{27}$$

where $\boldsymbol{A}_d' = \boldsymbol{A}_d^{-1}$ and $\boldsymbol{M}' = \boldsymbol{A}_d^{-1}\boldsymbol{M}(\boldsymbol{A}_d^{-1})^\top$.

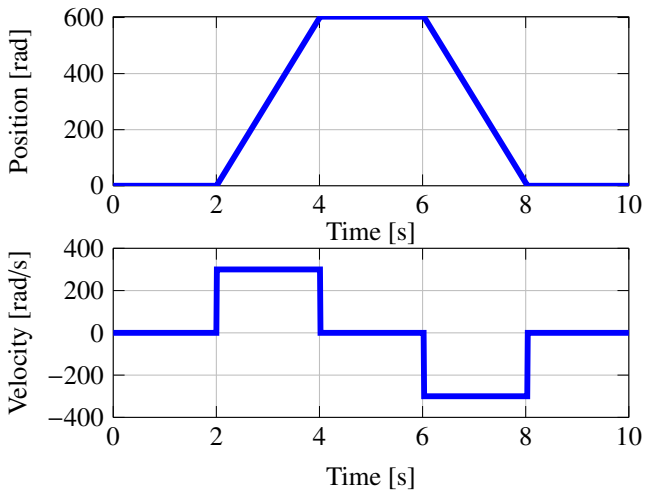

Fig. 3. State trajectory $\boldsymbol{r}_x$ for the second order system.

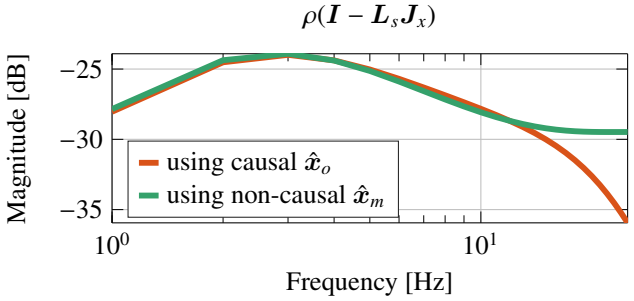

Fig. 4. Convergence condition of the state-tracking ILC assuming $\boldsymbol{Q}_s = \boldsymbol{I}_n$. Results of using a causal state observer (—) and non-causal state observer (—) are shown.

Proof. Due to calculating the state estimation backwards as in (26), state matrix of the system and covariance of the system noise become, $\boldsymbol{A}_d^{'} = \boldsymbol{A}_d^{-1}$ and $\boldsymbol{M}^{'} = \boldsymbol{A}_d^{-1}\boldsymbol{M}(\boldsymbol{A}_d^{-1})^\top$, respectively. □

4.4 Composition of the estimations

The non-causal state estimation $\hat{\boldsymbol{x}}_m$ is obtained by combining the forward estimation $\hat{\boldsymbol{x}}_f$ obtained in Section 4.2 and the backward estimation $\hat{\boldsymbol{x}}_b$ obtained in Section 4.3. The composition is done based on the covariance matrix of both state estimation errors. Defining a splitting ratio

$$\mathfrak{S} = \boldsymbol{P}_b(\boldsymbol{P}_f + \boldsymbol{P}_b)^{-1}, \tag{28}$$

the non-causal state estimation $\hat{\boldsymbol{x}}_m$ is composed by

$$\hat{\boldsymbol{x}}_m = \mathfrak{S}\hat{\boldsymbol{x}}_f + (\boldsymbol{I} - \mathfrak{S})\hat{\boldsymbol{x}}_b. \tag{29}$$

For proof of $\mathfrak{S} = \boldsymbol{P}_b(\boldsymbol{P}_f+\boldsymbol{P}_b)^{-1}$ being the most optimal splitting ratio, see literature Simon (2006).

5. SIMULATION VALIDATION

In this section, the performance of the state-tracking ILC utilizing the non-causal state observer is presented. The performance is compared with the previous state-tracking ILC which uses a causal state observer. In Section 5.3, the improved on-sample state tracking is demonstrated.

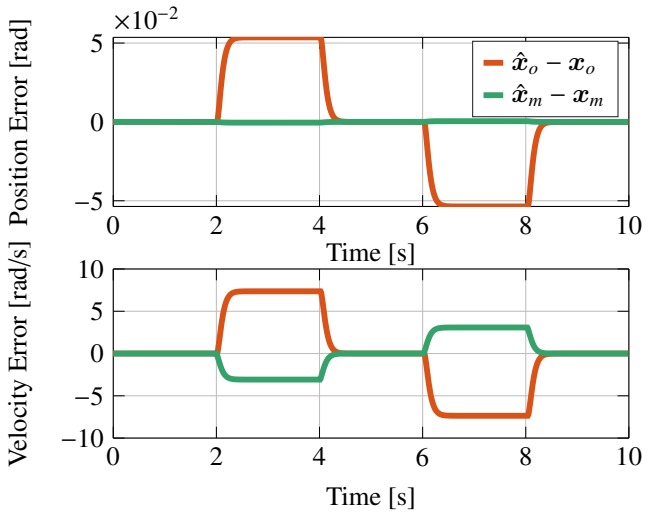

Fig. 5. Simulation results of the state estimation error of a causal observer (—) and the non-causal observer (—). In the 1st iteration when only feedback is applied, $\boldsymbol{x}_o = \boldsymbol{x}_m$ holds.

5.1 Simulation setup and approach

For simulation, a second order system $G = \frac{17699}{s(s+32.04)}$ with sampling time $T_s = 0.01$ s and a continuous time reference r shown in Fig. 3 is considered. The discretized system by zero-order-hold is $G_d = \frac{0.79756(z+0.8988)}{(z-1)(z-0.7259)}$. When the nominal plant and feedback controller are respectively $G_n = \frac{0.82224(z+0.9022)}{(z-1)(z-0.7341)}$ and $K_d = \frac{0.016365(z-0.7653)}{(z-0.746)}$, assuming the controllable canonical form, the state reference and state are given as $\boldsymbol{r}_x = [r, \dot{r}]^\top$ and $\boldsymbol{x} := [x_1, x_2]^\top = [y, \dot{y}]^\top$ respectively.

For the state observer, the covariance matrix of the system noise and measurement noise are set to $\boldsymbol{M} = \mathrm{diag}(10^{-6}, 1)$, $N = 10^{-6}$. From Example 1, the bandwidth of the state observer is 37 Hz. In this simulation, results of state-tracking ILC using a causal state observer $\hat{\boldsymbol{x}}_o$ and the proposed non-causal state observer $\hat{\boldsymbol{x}}_m$ are compared.

From Section 2.1, the learning filter is constructed based on the nominal plant information to achieve $\boldsymbol{L}_s = \boldsymbol{J}_x^{-1}$. For perfect state-tracking, $\boldsymbol{Q}_s = \boldsymbol{I}_n$ is desired (Lemma 4) and from Fig. 4 the convergence condition shows that such robustness filter is applicable for both cases.

Learning gain $\alpha = 0.5$ is exploited to mitigate the amplification of the time-varying disturbance (Oomen and Rojas, 2017) by replacing (7) as

$$\underline{f}_{j+1} = \boldsymbol{Q}_s(\underline{f}_j + \alpha\boldsymbol{L}_s\boldsymbol{e}_{\hat{\boldsymbol{x}},j}), \tag{30}$$

and for each ILC, 30 iteration learning is performed.

5.2 Improved state estimation

Fig. 5 shows the state estimation results of the two methods in the 1st iteration, when only feedback is applied. This figure shows that by effectively utilizing the non-causality, the non-causal state observer outperforms the causal state observer in state estimation. As mentioned in Section 2.2, the performance of state-tracking ILC depends on the accuracy of state estimation. Therefore, Fig. 5 directly indicates the final state-tracking error of both state-tracking ILC, shown in the later Fig. 7.

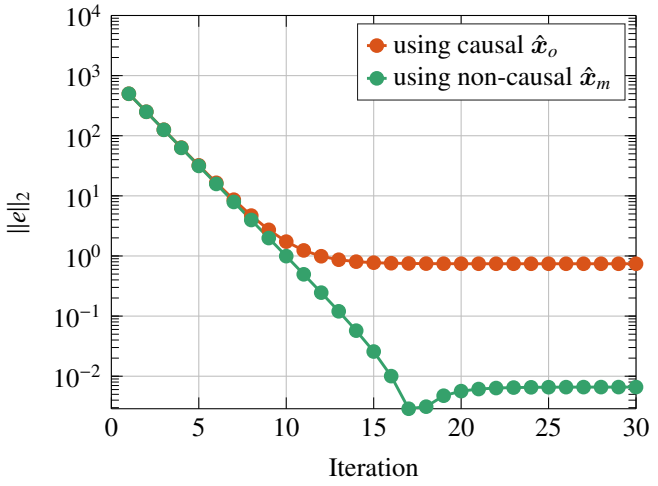

Fig. 6. Simulation results of the tracking error of state-tracking ILC. State-tracking ILC using the non-causal state observer (●) outperforms the state-tracking ILC using only a causal state observer (●).

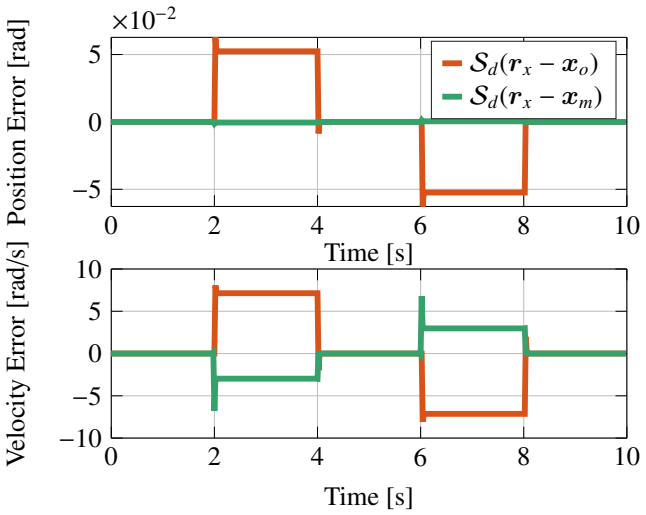

Fig. 7. Tracking error comparison of the 30th iteration. The dots are plotted for each 2 samples. The proposed state-tracking ILC using the non-causal state observer (▬) is showing better on-sample state tracking results than previous method using only a causal state observer (▬).

5.3 Improved on-sample state tracking performance

Fig. 6 shows the norm comparison of the two methods and it shows that the proposed state-tracking ILC using the non-causal state observer outperforms the previous state-tracking ILC using the causal state observer. In the final iteration, the norm of tracking error is reduced by 99.1%. Fig. 7 shows the tracking error comparison of the final iteration. From the result, due to better state estimation by the non-causal state observer, $\hat{x}_m$ becomes closer to the actual state x, resulting to a better state tracking error.

6. CONCLUSION

The developed non-causal state estimation framework fits the last remaining piece of non-causality which can be implemented to state-tracking ILC. Due to making full use of data, a more precise state estimation can be achieved without compromising the noise sensitivity. Application to a second order system and the validation demonstrate a superior on-sample state-tracking performance over the previous state-tracking ILC, by utilizing the improved state estimation yielded from the non-causal state observer.

REFERENCES

Anderson, B.D.O. and Moore, J.B. (2005). *Optimal Filtering*. Courier Corporation.

Bristow, D.A. and Tharayil, M. and Alleyne, A.G. (2006). A survey of iterative learning control. *Control Systems, IEEE*, 26(3), 96–114.

Csencsics, E., Ito, S., Schlarp, J., and Schitter, G. (2019). System integration and control for 3D scanning laser metrology. *IEEJ Journal of Industry Applications*, 8(2), 207–217.

Fujimoto, H., Hori, Y., and Kawamura, A. (2001). Perfect Tracking Control Based on Multirate Feedforward Control with Generalized Sampling Periods. *IEEE TRANSACTIONS ON INDUSTRIAL ELECTRONICS*, 48(3), 636–644.

Hayashi, T., Fujimoto, H., Isaoka, Y., and Terada, Y. (2020). Projection-based iterative learning control for ball-screw-driven stage with consideration of rolling friction compensation. *IEEJ Journal of Industry Applications*, 9(2), 132–139.

Mishra, S., Coaplen, J., and Tomizuka, M. (2007). Precision positioning of wafer scanners segmented iterative learning control for nonrepetitive disturbances. *Control Systems, IEEE*, 27(4), 20–25.

Norrlöf, M. and Gunnarsson, S. (2002). Time and frequency domain convergence properties in iterative learning control. *International Journal of Control*, 75(14), 1114–1126.

Ohnishi, W., Beauduin, T., and Fujimoto, H. (2019). Preactuated Multirate Feedforward Control for Independent Stable Inversion of Unstable Intrinsic and Discretization Zeros. *IEEE/ASME Transactions on Mechatronics*, 24(2), 863–871.

Ohnishi, W., Strijbosch, N., and Oomen, T. (2021). Multirate state tracking for improving intersample behavior in iterative learning control. In *2021 IEEE International Conference on Mechatronics (ICM)*, 01–06.

Oomen, T. (2018). Advanced Motion Control for Precision Mechatronics: Control, Identification, and Learning of Complex Systems. *IEEJ Journal of Industry Applications*, 7(2), 127–140.

Oomen, T. and Rojas, C.R. (2017). Sparse iterative learning control with application to a wafer stage: Achieving performance, resource efficiency, and task flexibility. *Mechatronics*, 47, 134–147.

Simon, D. (2006). *Optimal state estimation: Kalman, H∞, and nonlinear approaches*. John Wiley & Sons.

Van Der Meulen, S.H., Tousain, R.L., and Bosgra, O.H. (2008). Fixed structure feedforward controller design exploiting iterative trials: Application to a wafer stage and a desktop printer. *Journal of Dynamic Systems, Measurement and Control, Transactions of the ASME*, 130(5), 0510061–05100616.

Van Zundert, J. and Oomen, T. (2018). On inversion-based approaches for feedforward and ILC. *Mechatronics*, 50, 282–291.

Wallén, J., Norrlöf, M., and Gunnarsson, S. (2011). A framework for analysis of observer-based ILC. *Asian Journal of Control*, 13(1), 3–14.